

Supplementary Material

AMS Data Processing. AMS data were saved in 150-s intervals in alternating medium- and high-resolution modes [DeCarlo *et al.*, 2006]. The AMS data were processed using the software toolkit “Squirrel” with the “Pika” module,¹ including several updates to the fragmentation table [Allan *et al.*, 2004]. Specifically, the fragmentation coefficients at m/z 16, 17, 18, 29, 30, 39, 40, 44, and 46 were adjusted to account for the variability of gas-phase contributions and for the interference of ions having the same nominal m/z . Air contributions (e.g., $^{15}\text{NN}^+$ at m/z 29) were subtracted based on the data recorded with a HEPA filter in-line. Variations of the CO_2^+ signal at m/z 44 were corrected using measured gas-phase CO_2 concentration. The signals of CO^+ at m/z 28 and organic H_xO^+ at m/z 16, 17, and 18 were adjusted using the approach of Aiken *et al.* [2008]. The signals of NH_2^+ at m/z 16, NH_3^+ at m/z 17, NO^+ at m/z 30, NO_2^+ at m/z 46, and Ar^+ at m/z 40 were calculated as time-dependent fractions of the signals at unit resolution. C_3H_3^+ at m/z 39, which made up about 5% of the total organic signal, was calculated based on the ratio of C_3H_3^+ to Ar^+ .

The campaign-average loading of organic material (OM) was $0.7 \pm 0.3 \mu\text{g m}^{-3}$ ($< 1 \mu\text{m}$). This value is at the low end of the range of 1.0 to $2.0 \mu\text{g m}^{-3}$ reported in the previous campaigns ($< 2.5 \mu\text{m}$) [Graham *et al.*, 2003, and references therein; Fuzzi *et al.*, 2007]. In this comparison, a factor (OM:OC ≈ 1.7 [Fuzzi *et al.*, 2007]) is used by us for the conversion of OC reported in the previous studies to OM measured by the AMS. This OM:OC value is confirmed by the AMS result for AMAZE-08. Plausible explanations for the lower values reported herein include that approximately 30% of the fine-fraction OM measured in the previous studies was present in a size range of 1 to 2 μm , which lies

¹ <http://cires.colorado.edu/jimenez-group/ToFAMSResources/ToFSoftware/>.

outside the AMS measurement window, and that there were stronger influences from dust events and biomass burning in some of the previous studies not conducted in the middle of wet season and in other locations of the Amazon Basin.

Model Simulation. The GEOS-Chem global chemical transport model² was driven by GEOS-5 assimilated meteorology from the NASA Global Modeling and Assimilation Office. This model (v8.01.04) was employed here at a $2^\circ \times 2.5^\circ$ horizontal resolution. Fossil fuel and biofuel emissions of organic carbon were as described by *Park et al.*[2003]. Daily biomass burning emissions were obtained by applying emission factors from *Andreae and Merlet* [2001] to estimate the daily burned area, as calculated from the Rapid Response MODIS product [*Justice et al.*, 2002; *Giglio et al.*, 2003] and the MODIS Vegetation Continuous Fields [*Hansen et al.*, 2003] for 2008, in an approach similar to that of *Wiedinmyer et al.*[2006]. We assumed that 50% of the emitted organic particles from combustion sources was hydrophobic, with an e-folding conversion of 1.2 days from hydrophobic to hydrophilic [*Cooke et al.*, 1999]. Organic particle mass loading resulting from secondary-organic-aerosol production from the oxidation of monoterpenes, isoprene, and other volatile organic compounds followed the two-product model of *Chung and Seinfeld* [2002] that is based on empirical fits to environmental chamber data. The simulated organic-carbon concentrations were scaled by a factor of two to account for additional non-carbon mass (i.e., OM:OC = 2) to obtain the simulated organic particle mass loadings. Coarse-mode PBAPs that can make a large contribution to PM₁₀ mass loading were not included in the simulation and also are not measured by the AMS.

² <http://www-as.harvard.edu/chemistry/trop/geos>

Literature Cited

- Aiken, A. C., et al. (2008), O/C and OM/OC ratios of primary, secondary, and ambient organic aerosols with high-resolution time-of-flight aerosol mass spectrometry, *Environ. Sci. Technol.*, *42*, 4478-4485.
- Allan, J. D., et al. (2004), A generalised method for the extraction of chemically resolved mass spectra from aerodyne aerosol mass spectrometer data, *J. Aerosol Sci.*, *35*, 909-922.
- Andreae, M. O., and P. Merlet (2001), Emission of trace gases and aerosols from biomass burning, *Global Biogeochem. Cycles*, *15*, 955-966.
- Chung, S. H., and J. H. Seinfeld (2002), Global distribution and climate forcing of carbonaceous aerosols, *J. Geophys. Res.*, *107*(D19), doi:10.1029/2001JD001397.
- Cooke, W. F., C. Liousse, H. Cachier, and J. Feichter (1999), Construction of a 1 degrees x 1 degrees fossil fuel emission data set for carbonaceous aerosol and implementation and radiative impact in the ECHAM4 model, *J. Geophys. Res.*, *104*, 22137-22162.
- DeCarlo, P. F., et al. (2006), Field-deployable, high-resolution, time-of-flight aerosol mass spectrometer, *Anal. Chem.*, *78*, 8281-8289.
- Fuzzi, S., et al. (2007), Overview of the inorganic and organic composition of size-segregated aerosol in Rondonia, Brazil, from the biomass-burning period to the onset of the wet season, *J. Geophys. Res.*, *112*, D01201, doi:10.1029/2005JD006741.
- Giglio, L., J. Descloitres, C. O. Justice, and Y. J. Kaufman (2003), An enhanced contextual fire detection algorithm for MODIS, *Remote Sens. Environ.*, *87*, 273-282.
- Graham, B., et al. (2003), Composition and diurnal variability of the natural Amazonian aerosol, *J. Geophys. Res.*, *108*(D24), 4765, doi:10.1029/2003JD004049.
- Hansen, M., R. S. DeFries, J. R. G. Townshend, M. Carroll, C. Dimiceli, and R. A. Sohlberg (2003), Global Percent Tree Cover at a Spatial Resolution of 500 Meters: First Results of the MODIS Vegetation Continuous Fields Algorithm, *Earth Interact.*, *7*, 1-15.
- Justice, C. O., et al. (2002), The MODIS fire products, *Remote Sens. Environ.*, *83*, 244-262.
- Park, R. J., D. J. Jacob, M. Chin, and R. V. Martin (2003), Sources of carbonaceous aerosols over the United States and implications for natural visibility, *J. Geophys. Res.*, *108*(D12), doi:10.1029/2002JD003190.
- Wiedinmyer, C., et al. (2006), Estimating emissions from fires in North America for air quality modeling, *Atmos. Environ.*, *40*, 3419-3432.

Table S1. Mean percent contributions of intense peaks to the total organic particle mass loadings in the 12-h averaged mass spectra. These peaks contribute more than 40% of the total organic loading for all classes. One standard deviation is shown in parentheses as a percentage of the mean contribution.

<i>m/z</i>	27	29	39	41	42	43	44	53	55	91
Ion Type	C ₂ H ₃ ⁺	C ₂ H ₅ ⁺ CHO ⁺	C ₃ H ₃ ⁺	C ₃ H ₅ ⁺	C ₂ H ₂ O ⁺	C ₂ H ₃ O ⁺	CO ₂ ⁺	C ₄ H ₅ ⁺	C ₄ H ₇ ⁺ C ₃ H ₃ O ⁺	C ₇ H ₇ ⁺
Class I	4.3 (3.2%)	5.4 (18%)	4.9 (5.2%)	3.9 (4.2%)	3.1 (3.2%)	9.6 (5.9%)	9.1 (4.9%)	1.8 (6.5%)	2.5 (4.6%)	0.8 (7.7%)
Class II	4.4 (8.6%)	3.7 (68%)	4.8 (10%)	3.0 (62%)	3.0 (8.1%)	8.4 (11%)	11 (8.5%)	1.9 (11%)	2.2 (6.5%)	0.6 (13%)
Class III	4.1 (9.6%)	3.6 (9.4%)	4.3 (15%)	2.6 (42%)	2.7 (12%)	6.9 (14%)	13 (6.2%)	1.8 (16%)	2.0 (6%)	0.5 (25%)

List of Figures

Figure S1. Histogram of sulfate mass fraction obtained by AMS measurements during AMAZE-08. Bars represent 12-h averages. The dashed line represents the original 150-s data.

Figure S2. (a, b) Diel profiles of the ratio of the organic m/z 44 to m/z 43 during class I and III periods. (c, d) Diel profiles of sulfate mass loadings during class I and III periods. Although the autocorrelation within the classification time series is significant (not shown), these classes are nevertheless defined by this mode criterion and do not correspond directly to contiguous or sequential blocks of time during AMAZE-08. The low loading (Fig. 3b) as well as low ratio of the organic m/z 44 to m/z 43 at sunrise for class III periods was plausibly explained by the previous non-class III time blocks.

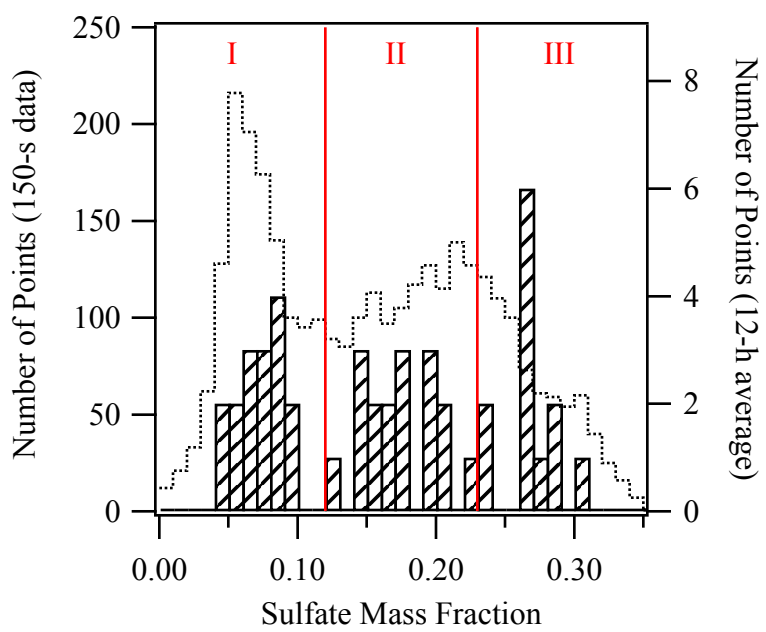


Figure S1.

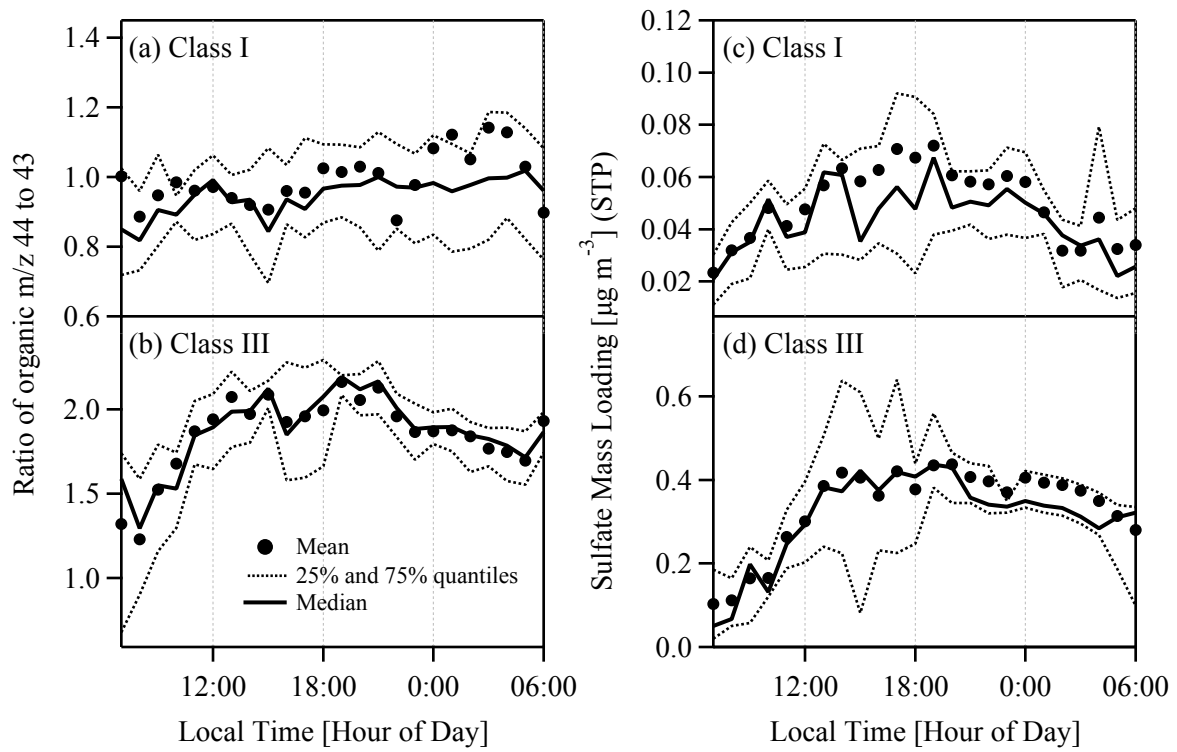


Figure S2.